

## FABRY-PÉROT ABSORPTION LINE SPECTROSCOPY OF THE GALACTIC BAR. II. STELLAR METALLICITIES

NASEEM RANGWALA<sup>1</sup> AND T. B. WILLIAMS<sup>1,2</sup>

*Accepted for publication in the Astrophysical Journal June 26, 2009*

### ABSTRACT

We measure the Ca II  $\lambda 8542$  line strength in 3360 stars along three lines-of-sight in the Galactic bar:  $(l, b) \sim (\pm 5.0, -3.5)^\circ$  and Baade's Window, using FP absorption line spectroscopy. This is the first attempt to show that reliable absorption line strengths can be measured using FP spectroscopy. The Ca II  $\lambda 8542$  line is a good indicator of metallicity and its calibration to  $[\text{Fe}/\text{H}]$  is determined for globular cluster red giants in previous investigations. We derive such a calibration for the bulge giants and use it to infer metallicities for our full red clump sample (2488 stars) at all three lines-of-sight. We present the stellar metallicity distributions along the major axis of the bar. We find the mean  $[\text{Fe}/\text{H}] = -0.09 \pm 0.04$  dex in Baade's Window, and find the distribution in this field to agree well with previous works. We find gradients in the mean metallicity and its dispersion w.r.t Baade's Window of  $-0.45$  and  $-0.20$  dex respectively at  $l = +5.5^\circ$  and of  $-0.10$  dex and  $-0.20$  dex at  $l = -5.0^\circ$ . We detect a signature of a possible tidal stream at  $l = +5.5^\circ$ , in both our velocity and metallicity distributions. Its radial velocity indicates that it is not associated with the Sagittarius stream. We also measure the metallicity of a bulge globular cluster NGC 6522 in our Baade's Window field to be  $-0.90 \pm 0.10$  dex, in agreement with recent measurements of Zoccali et al. (2008). This agreement demonstrates the reliability of our metallicity measurements.

*Subject headings:*

### 1. INTRODUCTION

This is the second paper of the series on measurements of radial velocities and equivalent widths using the Ca II  $\lambda 8542$  line for a large sample of stars in the Galactic bar, based on Fabry-Pérot (FP) absorption line spectroscopy. In Paper I (Rangwala et al. 2009), we used FP imaging spectroscopy at three lines-of-sight (LOS) in the bar:  $(l, b) \sim (\pm 5, -3.5)$  and Baade's Window (BW) to obtain a total of 2488 bar red clump giants (RCGs), 339 bar M giants (red giant branch), and 318 disk main sequence stars. This sample is an order of magnitude larger than any previous sample for a given LOS.

The existence of a bar in the Milky Way (MW) is now firmly established. Its photometric signature is seen as a distinct peanut-shaped bulge in the COBE maps (Dwek et al. 1995; Freudenreich 1998). The signature of the bar is also confirmed in the bulge red clump giant (RCG) population (Stanek et al. 1997), in microlensing (Alcock et al. 2000), and in stellar and gas kinematics (Howard et al. 2008; Rangwala et al. 2009; Weiner & Sellwood 1999). These morphological and dynamical observations strongly indicate a bar-like feature, formed from secular evolution processes. But detailed chemical abundance measurements (Rich 1988; Matteucci 1992; Ballero et al. 2007; Zoccali et al. 2007) in Baade's Window find an old,  $\alpha$ -enhanced, and metal-rich population, indicating a bulge that was formed on a very short timescale with high star formation efficiency. To understand and resolve the issues related to the formation of structure in the inner Galaxy, a variety of dynamical and chemical studies have been performed over many years and still continue. For recent progress in the studies of the Galactic bulge see the reviews by Minniti & Zoccali (2008) and Rich et al. (2007).

In Paper I, we showed that FP techniques are very efficient for simultaneously measuring high precision radial velocities of a large sample of stars. Our large radial velocity sample produced an accurate determination of the detailed shape of this velocity distribution in the bar and measured the difference in the radial streaming motions of the stars on the near and far sides of the bar. These observations provide strong constraints on the dynamical models of the bar (Debattista et al. in preparation).

The main goal of this paper is to test the suitability of FP spectroscopy for reliable and robust line strength measurements, and to determine the stellar metallicity distributions along the three LOS. The calcium triplet (CaT) lines in the cool giants have been established as reliable indicators of  $[\text{Fe}/\text{H}]$ , and have been used extensively to infer the metallicities of globular clusters (Armandroff & Zinn 1988; Armandroff & Da Costa 1991; Zinn 1985; Rutledge et al. 1997; Cole et al. 2004; Carrera et al. 2007) and of dwarf spheroidal galaxies (Tolstoy 2005). These investigations have determined the calibration between the summed equivalent widths of the triplet and  $[\text{Fe}/\text{H}]$  using red giants in numerous globular clusters (GC) over a range of  $[\text{Fe}/\text{H}]$  ( $-2.0 \lesssim [\text{Fe}/\text{H}] \lesssim +0.5$  dex). We can apply similar techniques to use our Ca II  $\lambda 8542$  line strength measurements to obtain  $[\text{Fe}/\text{H}]$  for our large sample of stars. We demonstrate the

<sup>1</sup> Department of Physics and Astronomy, Rutgers University, 136 Frelinghuysen road, Piscataway, NJ 08854

<sup>2</sup> Visiting astronomer, Cerro Tololo Inter-American Observatory, National Optical Astronomy Observatory, which are operated by the Association of Universities for Research in Astronomy, under contract with the National Science Foundation.

reliability of our EWs by measuring the mean  $[\text{Fe}/\text{H}]$  of NGC 6522, a bulge globular cluster that is present in our BW field. We also determined a new calibration between the CaT index and  $[\text{Fe}/\text{H}]$  for the bulge RCGs by using recent high resolution  $[\text{Fe}/\text{H}]$  measurements by Zoccali et al. (2007), and apply this calibration to infer metallicity for our sample.

Measuring the stellar metallicity distribution (SMD) from a large sample of stars can be a very useful tool for the chemical evolution models to constrain different formation scenarios for the bulge (e.g. Did it form inside-out or outside-in? What is the timescale of its formation?). The SMD in BW has been measured by many authors using both high and low-resolution spectroscopy and photometric data (Sadler et al. 1996; Fulbright et al. 2006; Zoccali et al. 2003, 2007). These measurements in BW find the bulge to be metal-rich and  $\alpha$ -enhanced, supporting the formation model where the bulge was formed on a short timescale (less than a Gyr) with a high star-formation rate (Ballero et al. 2007). If there is a bar and a classical bulge then abundance studies in BW alone will not be sufficient to separate the two components. Looking for metallicity gradients along the bar can provide additional constraints on differences between the two components. Our measurements differ from previous works both in the large sample size and in including two positions along the major axis of the bar in addition to BW.

The combination of velocity and metallicity distributions can be used to detect the signature of tidal streams associated with disrupted satellites. The Sagittarius stream was discovered in the measurements of the bulge velocity distribution by Ibata et al. (1995). We report in this paper an indication of a possible tidal stream at our  $l = +5.5^\circ$  LOS.

## 2. OBSERVATIONS AND DATA REDUCTION

The observations were made using the Rutgers Fabry-Pérot system on the CTIO 1.5m telescope. A total of 10 sub-fields were observed: four each at  $l \simeq \pm 5^\circ$  (MM7B and MM5B fields respectively) and two in BW. The positions of these fields are listed in Table 1 of Paper I. We chose to observe the Ca II  $\lambda 8542$  line, which is one of the strongest features in the late-type stars like the RCGs, is not contaminated by the foreground ISM, and is relatively free of strong terrestrial emission lines. We used a medium-resolution etalon with a spectral response function that is well fit by a Voigt function with a FWHM of 4 Å, equivalent to approximately 140 km s<sup>-1</sup> at 8500 Å. We typically scanned a range of 8530 – 8555 Å with wavelength steps of 1 Å.

The basic procedure in Fabry-Pérot (FP) imaging spectroscopy is to obtain a series of narrow-band images, tuning the interferometer over a range of wavelengths covering a spectral feature of interest. The data cube thus produced is analyzed to extract a short portion of the spectrum of each object in the field of view, using DAOPHOT (Stetson 1987) to measure a flux of each star in each image. For a field of view with many objects of interest, the technique can be extremely efficient. For example, in this work we obtained about 500 stars per data cube for our 4' field of view.

The Ca II  $\lambda 8542$  absorption line is fit with a Voigt function to obtain the central wavelength, continuum, total area in the line, and the Gaussian and Lorentzian widths. A sub-sample of our spectra are shown in Figure 2, illustrating the range of equivalent widths (EW) measured. Our sample for three LOS consists a total of 2488 bar RCGs,  $\sim 300$  bar M-giants and  $\sim 350$  disk main sequence stars. To select these various stellar populations we used I and V band photometry, the majority of which comes from the OGLE catalogue (Szymanski 2005). The selections are shown in Figure 1 (left panel) and discussed in Paper I. As shown in Cenarro et al. (2001), in later-type M-giants a TiO band distorts the continuum around the calcium triplet, and strongly affects the measured equivalent width of the lines. Our color selection limits our sample to K-giants, and avoids this effect.

The right panel of Figure 1 shows the uncertainties of the EW measurements over the S/N range of our sample. The median fractional uncertainty is 1/6th of the EW. As expected, the uncertainty increases when the S/N decreases, but there is a wide uncertainty range at S/N  $\sim 20$ , which comes mostly from sampling different portions of the line in different stars (see Figure 2). Another source of uncertainty comes from the fact that we observe a limited part of the spectrum around the Ca II  $\lambda 8542$  line compared to slit spectra, which typically measure the entire line profile and surrounding continuum. To investigate the effects of our limited spectral range, we generate 1000 random realizations of the spectrum of each of 8 red giants from the globular cluster 47 Tuc (provided by Andrew Cole; private comm.). We fit Voigt functions to these spectra over two different bandpasses: 25 Å (FP) and 60 Å (slit). The mean EW and standard deviation for each of the 8 stars is plotted in Figure 3. No bias is introduced in the EW due to the limited FP bandpass, but the uncertainty is larger by a factor of 1.5.

We only measure the single, strongest line of the triplet. The total EW of all three lines is  $\sum W = W_{8498} + W_{8542} + W_{8662} = 2.21W_{8542}$ . The factor of 2.21 is verified using the data from 47 Tuc and was also confirmed by Andrew Cole (private comm.), who finds this factor to be the same over a wide range of metallicities. This factor is also consistent with synthetic spectra, the solar spectrum (Mould 1976), and the spectra of many dwarf and giant stars (Jones et al. 1984).

## 3. MEASUREMENT OF EQUIVALENT WIDTH AND COMPARISON WITH DIFFERENT INDICES

In Paper I, we published measurements of the EW of the Ca II  $\lambda 8542$  line by fitting a Voigt function to the absorption line and integrating the fit over all wavelengths. We call this index  $W_\infty$  to indicate that the integration bandpass is from 0 to  $\infty$ . Our spectra are measured over a limited wavelength range, which could affect the continuum and EW measurements. In addition we need to assess the effects of our  $W_\infty$  definition, which differs from the indices used in previous investigations. We use both the synthetic spectral line database of Munari et al. (2005)<sup>3</sup> and also spectra of

<sup>3</sup> <http://archives.pd.astro.it/2500-10500/>

the red giants from 47 Tuc to analyze these effects.

We compare our index to those of Cole et al. (2004) (C04 hereafter) and Carrera et al. (2007) (Ca07 hereafter). C04 measure the EW of all three of the calcium triplet lines, fitting each with the sum of a Gaussian and a Lorentzian, and then integrating the fit over a 20 Å bandpass. Ca07 use the same functional form as C04 but different, and wider continuum and line bandpasses<sup>4</sup>. Ca07 found no significant differences between their index and that of C04, but we will show below that there is a small systematic difference between them. These two indices differ from  $W_\infty$  in three ways: the functional form, the continuum definition, and the integration bandpass. We address the effects of each of these factors below.

We created a series of artificial profiles using a Voigt function with a range of Gaussian and Lorentzian widths, and then fitted them with the sum function. In every case the sum fit is indistinguishable from the Voigt profile and yields the same EW. We also verified that fitting the 47 Tuc spectra with the two functional forms gives identical profiles and EW. We conclude that the value of the EW index is independent of the choice between these two functional forms. We choose to use the Voigt function because the intrinsic stellar line profile is a Voigt, our instrumental profile is a Voigt, and the convolution of the two is also a Voigt.

We generate synthetic spectra with the following stellar parameters:  $T_{\text{eff}} = 4750$  K,  $\log(g) = 3.0$  (in  $\text{cm s}^{-2}$ ),  $V_{\text{rot}} = 5$   $\text{km s}^{-1}$ , micro-turbulence = 2  $\text{km s}^{-1}$  and  $[\alpha/\text{Fe}] = 0.0$ . These values are consistent with Zhao et al. (2001)'s high-resolution spectroscopic measurements of the red clump giants in the solar neighborhood. Synthetic spectra were obtained for  $[\text{Fe}/\text{H}] = [-2.0, -1.5, -1.0, -0.5, 0.0, +0.5]$  dex, covering the entire range of metallicities available in the database. We then convolve these synthetic spectra with our instrumental profile, a Voigt of  $\sim 4$  Å FWHM.

We fit the Ca II  $\lambda 8542$  line in the synthetic spectra with a Voigt function in two ways: first, in which the continuum is measured as the mean flux within several bands, using exactly the same procedure and definition as Ca07, and second, in which the continuum is one of the parameters of the Voigt function fit over a 25 Å bandpass from 8530 – 8555 Å to simulate our FP spectra. We fitted the spectra for all available metallicities (listed above), and show the fits for the highest and lowest  $[\text{Fe}/\text{H}]$  in Figure 4. The solid and dotted lines show the fits with the two different continuum definitions. The continuum windows of Ca07 are shown by vertical dashed lines. The differences in the two continuum levels are about 0.4% and 0.7% for the low and high  $[\text{Fe}/\text{H}]$ , respectively and the FP-fit continuum is always lower than the Ca07 continuum. For an integration bandpass of 40 Å the continuum difference would produce an EW difference of less than 0.3 Å in even the strongest-lined stars. We will neglect this systematic difference, both because our random errors are relatively large (median error  $\sim 0.7$  Å), and because our calibration will compensate for systematic effects.

Since the choice of fitting function and the continuum definition have at most a minor effect on the line index, the choice of integration bandpass is the major contributor to the systematic differences between the index values. Collisional or pressure broadening in the stars atmospheres gives rise to strong damping wings on the calcium line absorption profiles. In metal rich stars, as much as 75% of the EW comes from the wings (Erdelyi-Mendes & Barbuy 1989), and in the Sun the wings extend out to at least 30 Å on either side of the line center (Smith & Drake 1988). Thus we expect that the measured values of the line indices will depend strongly on the spectral range over which the fitted profiles are integrated. We will denote the bandpass definitions of C04 and Ca07 by  $W_{20}$  and  $W_{40}$  respectively, and our integration of the entire profile as  $W_\infty$ . Figure 5 compares these indices for the Ca II  $\lambda 8542$  line, measured in synthetic spectra with a range of metallicities, and also in the observed spectra of 8 red giants in 47 Tuc. Broader integration bandpasses produce systematically larger EW index values, and these differences increase with line strength (or metallicity). In the left panel of Figure 6 we show the measured equivalent width of the Ca II  $\lambda 8542$  line in one of the 47 Tuc stars as a function of integration bandpass. The first two points in the plot show  $W_{20}$  and  $W_{40}$ , respectively. The EW converges to  $W_\infty$  for bandpasses greater than 200 Å.

In the middle panel of Figure 6 we compare the values of  $W_\infty$  and  $W_{40}$ , measured for our entire sample of FP spectra at  $l = -5^\circ$ . As expected from the tests shown in Figure 5, there is a tight, but non-linear, relation between the indices. We overplot the indices from the synthetic spectra of Figure 5a, showing that the indices measured from the limited-range FP data are in excellent agreement with those measured from more extensive, traditional spectra. We have used Monte Carlo simulations to estimate the uncertainties of  $W_\infty$  and  $W_{40}$  in the fits to our FP data, and find that the fractional uncertainties of the two indices are identical. Thus it seems to make little difference which integration bandpass one chooses to use. Of course, to apply a previously-determined calibration of the CaT index to  $[\text{Fe}/\text{H}]$ , one must use the same index definition. In the right panel of Figure 6 we show the calibration of  $W_{20}$  for globular clusters as measured by C04. We use the  $W_\infty - W_{20}$  correlation to calculate the corresponding calibration relation for  $W_\infty$ , shown by the dotted curve.

#### 4. COMPARISON WITH HIGH-RESOLUTION METALLICITIES

##### 4.1. *Metallicity of NGC 6522*

NGC 6522 is a bulge globular cluster that appears at the southwest edge of our BW field (see Figure 2 of Paper I). The stars from this cluster show up as a distinct kinematic feature in our velocity distribution (see Figure 8 of Paper I). We can use the EWs of these stars to measure the mean metallicity of this cluster via the calcium infrared triplet method. We will compare our measurement to the most recent high-resolution  $[\text{Fe}/\text{H}]$  determination for this cluster

<sup>4</sup> The line and continuum bandpass used by Ca07 are defined in Cenarro et al. (2001)

by Zoccali et al. (2008) (Zoc08 hereafter), in order to assess the accuracy of our procedures.

To isolate possible members of this cluster from the background bulge population we use the kinematics and photometry of the cluster. We identify the red giant branch of this cluster from the HST CMD (Piotto et al. 2002) and select the stars within  $1\text{-}\sigma$  ( $7.9 \text{ km s}^{-1}$ ) of the cluster’s mean velocity ( $-14.67 \text{ km s}^{-1}$ ). We find 28 possible members of this cluster, majority of which fall within  $2'$  of the cluster center. Compared to the mean EW at a given  $V$  magnitude, the EW of three stars deviates significantly (one with a relatively large EW and two with relatively small EWs). Because the cluster’s velocity is very near the center of the bulge velocity distribution, the kinematic selection constrain cannot eliminate all of the bulge contamination. In addition, all three stars are near the faint end of the photometric distribution, where there is a higher probability of bulge contamination. We therefore exclude these three stars from the cluster sample. The three excluded stars are indicated by triangles in Figure 7.

To convert EWs to metallicity we follow the method in C04. For this analysis we will use  $W_{40}$  so that we can consistently use the calibration of C04 and compare to previous work. The first step is to measure the ‘reduced equivalent width’ to correct for the strong effects of stellar effective temperature and surface gravity in the red giants. This is given by:

$$W' = \sum W + \beta(V - V_{\text{HB}}) \quad (1)$$

where the introduction of the horizontal branch magnitude ( $V_{\text{HB}}$ ) removes dependence on the cluster distance or reddening, and  $\sum W = 2.21W_{40}$  is the summed EW of all three CaT lines. Figure 7 shows this relationship for  $V_{\text{HB}} = 16.85 \pm 0.20$  (Rutledge et al. 1997).  $\sum W$  increases linearly up the red-giant branch as expected. The best fit to the data is shown by the solid line with a slope of  $\beta = 0.71 \pm 0.22 \text{ \AA mag}^{-1}$ .

Within the  $1\text{-}\sigma$  error our slope is in good agreement with previous measurements of Rutledge et al. (1997), Ca07 and C04 who measured it to be  $0.64 \pm 0.02$ ,  $0.647 \pm 0.005$  and  $0.73 \pm 0.04$  respectively, using the data from numerous globular clusters.

The calibration between  $W'$  and  $[\text{Fe}/\text{H}]$  as measured by C04 is:

$$[\text{Fe}/\text{H}] = (-2.966 \pm 0.032) + (0.362 \pm 0.014)W' \quad (2)$$

This calibration has a rms scatter of  $\sigma = 0.07$  dex and is measured for metallicity range of  $-2.0 \lesssim [\text{Fe}/\text{H}] \lesssim +0.5$  dex (Carrera et al. 2007).

Using this calibration and  $W' = 5.70 \pm 0.15 \text{ \AA}$  (for  $V_{\text{HB}} = 16.85$ ) we obtain  $[\text{Fe}/\text{H}]_{\text{NGC6522}} = -0.90 \pm 0.10$  dex. For another value of  $V_{\text{HB}} = 16.52 \pm 0.07$  as measured from the HST CMD of Sosin et al. (1997) for this cluster we get  $W' = 5.96 \pm 0.15 \text{ \AA}$  and  $[\text{Fe}/\text{H}] = -0.81 \pm 0.10$  dex.

We compare this result with Zoc08 where they measure high-resolution abundances for stars in the Galactic bulge using VLT FLAMES-GIRAFFE spectrograph. Their sample consists of seven members from NGC 6522. The mean  $[\text{Fe}/\text{H}]$  from these seven stars is  $-0.91 \pm 0.06$  dex. Our measurement is in excellent agreement with this work. There is one star (OGLEID 412752) in common with both Zoc08 and our sample. For this star we get  $[\text{Fe}/\text{H}] = -0.84$  dex and  $-0.94$  dex ( $\pm 0.42$  dex) for lower and higher values of  $V_{\text{HB}}$  respectively, in agreement with  $-0.80 \pm 0.15$  dex as measured by Zoc08.

We also compare our result to Rutledge et al. (1997), who measured the calcium triplet index for 72 GCs. They get a lower  $[\text{Fe}/\text{H}]$  of  $-1.21 \pm 0.04$  using 9 possible members of this cluster. They use different weights for the EWs of the three calcium lines to get  $W' = 3.47 \pm 0.11$ . Converting our index to their system using Equation 3 of Ca07 we get  $W' = 4.08 \pm 0.12$ , which does not agree with Rutledge’s index. Our index converted to their system gives  $[\text{Fe}/\text{H}] = -0.91$  dex using their calibration between  $W'$  and  $[\text{Fe}/\text{H}]$ . Because NGC 6522 is a bulge cluster and has a velocity close to the mean of the bulge velocity distribution, it is very difficult to establish the membership for this cluster. From a sample of 11 stars that Rutledge et al. (1997) select as cluster members, 8 stars show velocity deviations larger than  $20 \text{ km s}^{-1}$  from the mean cluster velocity, suggesting that their sample may be significantly contaminated by bulge stars.

#### 4.2. Ca II $\lambda 8542$ – $[\text{Fe}/\text{H}]$ calibration for the bulge stars

There are 11 bulge giants in our sample that have high-resolution  $[\text{Fe}/\text{H}]$  measurements from Zoc08. We can use this sample to define a calibration between CaT and  $[\text{Fe}/\text{H}]$  for the bulge giants, and then use this calibration to infer  $[\text{Fe}/\text{H}]$  for the rest of our sample. We identify these stars as red clump giants, the metal-rich equivalent of horizontal branch stars, with a very narrow intrinsic luminosity distribution. We do not need to correct to ‘reduced equivalent width’ as we did for the cluster giants in the previous section. To support this assumption we plot in Figure 8  $W_{\infty}$  as a function of I-band magnitude (left panels) for our full RCG sample at all three LOS in the bar. There is no significant trend with luminosity. However, EW clearly does vary with the V-I color as shown in right panels of Figure 8. The slope of this relationship changes with the position along the bar, and is largest in BW. The 11 common stars are shown in red in Figure 8, and exhibit a similar trend in  $[\text{Fe}/\text{H}]$ , as shown in Figure 9(a). Thus the change in EW with color in the RCGs reflects a real trend in metallicity, and not a luminosity-dependent variation as seen on the red giant branch. Therefore we do not make any corrections in our sample for this trend.

One of the common stars (with OGLEID 423286) has an anomalously low EW for a given (V-I) color compared to the rest of the sample and will not be used in determining the calibration relation. We plot  $[\text{Fe}/\text{H}]$  from Zoc08 against our  $W_{40}$  for the 10 remaining stars in the right panel of Figure 9. The solid line shows the best straight-line fit to the data using the uncertainties in both coordinates.

The calibrations for  $W_{40}$  and  $W_{\infty}$  are:

$$[\text{Fe}/\text{H}] = (-3.828 \pm 0.131) + (0.475 \pm 0.154)(2.21 W_{40}) \quad (3)$$

and

$$[\text{Fe}/\text{H}] = (-3.545 \pm 0.125) + (0.384 \pm 0.114)(2.21 W_{\infty}) \quad (4)$$

Here we separate the factor 2.21 for converting single-line EW measurement to the summed EW of the triplet, to facilitate comparison with previous calibrations, e.g. Equation 2 above from C04.

This is the first determination of the CaT to  $[\text{Fe}/\text{H}]$  calibration for the bulge RCGs. All previous measurements were done using red giants in globular clusters. The dotted line in the right panel of Figure 9 shows the globular cluster calibration (Equation 2), which deviates from the bulge calibration at low and high metallicities. The reduced  $\chi^2$  for the globular cluster calibration is greater by 1.5, suggesting that the bulge calibration may not be the same as the globular cluster calibration.

Fulbright et al. (2007) show that the  $[\text{Ca}/\text{Fe}]$  ratio in bulge red giants varies from  $\sim 0.4$  dex to 0.0 dex as metallicity increases from  $[\text{Fe}/\text{H}] \sim -1.5$  to  $+0.0$  dex. Since our calibration is based on the bulge RCGs, it will automatically compensate for this effect. If the bulge and bar populations have different  $\alpha$ -element enhancements, and the ratio of these populations vary with position along the bar, then our calibration, derived in BW, could underestimate the metallicity at the  $l = \pm 5^\circ$  positions. Fulbright et al. (2007) show that the difference in  $\alpha$ -element enhancement between the bulge and the thick disk populations is about 0.2 dex, so the amplitude of this underestimate must certainly be less than this amount. Until high-resolution spectra are obtained for stellar samples at positions other than BW, it will be impossible to determine the exact change, if any, in the calibration relation along the bar. It is highly unlikely that the calibration changes by as much as 0.1 dex, an amount smaller than the uncertainty of the current calibration.

## 5. STELLAR METALLICITY DISTRIBUTIONS

We use  $W_{\infty}$  in Equation 4 to infer metallicities for the RCG sample (all the points shown in red in Figure 1) to obtain the SMDs at three LOS in the bar. The SMDs are shown in Figure 10. In the BW SMD (middle panel) a distinct peak around  $-0.90$  dex is from NGC 6522. The distribution is significantly broadened by our relatively large uncertainties. To take into account the effect of the individual errors we use maximum likelihood estimator (Pryor & Meylan 1993) to measure the true dispersion of these distributions. The mean and dispersion are listed in Table 1 along with the corresponding kinematics as measured in Paper I. Only statistical uncertainties are listed in this table. The calibration will introduce an additional systematic uncertainty of about 0.10 dex.

Previous observations of Fulbright et al. (2006) (also see Rich 1988; Sadler et al. 1996) show that the bulge metallicity distribution can range from  $-1.5$  to  $+1.0$  dex. Our SMDs have extended high metallicity tails that include  $\sim 12\%$  of the stars for each LOS. Most of the stars in these tails are at the faint end of our sample and have large EW uncertainties. Our calibrations extend only to  $[\text{Fe}/\text{H}] = +0.5$  dex, and the analysis of section 3 suggests that at higher metallicity the calibration may become non-linear. Thus we do not believe that our observations give reliable evidence for any stars with  $[\text{Fe}/\text{H}] \gtrsim 1.0$  dex. This conclusion is further supported by the comparison shown in Section 5.1 below, where SMDs with maximum  $[\text{Fe}/\text{H}] \lesssim 1.0$  dex, when convolved with our uncertainties, show similar extended tails.

The SMD at  $(l, b) = (5.5, -3.5)$  shows an excess at  $[\text{Fe}/\text{H}] = -1.0$  dex, significantly different from the mean  $[\text{Fe}/\text{H}]$  of the underlying distribution. The velocity distribution at this LOS from Paper I, reproduced here in the top panel of Figure 11, also shows an excess at  $V_{\text{los}} = -36.5 \text{ km s}^{-1}$ , about  $70 \text{ km s}^{-1}$  away from the mean of the distribution. Since our measurements of velocity are more accurate than those of metallicity, we select the stars between  $-45 \text{ km s}^{-1}$  and  $-28 \text{ km s}^{-1}$ , i.e. within one velocity standard deviation of the peak of this excess. This selection produces a sample of 47 stars. The metallicity distribution of these stars is shown in the bottom panel of Figure 11, where the peak at  $-1.0$  dex is much more evident. Other velocity selection limits produce similar metallicity distributions, with the peak becoming less striking as wider velocity limits are chosen. This feature may indicate the presence of a tidal stream or debris from a disrupted satellite.

Does this feature belong to the Sagittarius stream? The location and kinematics of the tidal debris of the Sagittarius dwarf galaxy have been traced by Majewski et al. (2004) and Martínez-Delgado et al. (2004). The Sagittarius stream passes through this LOS ( $l, b = 5.5, -3.5^\circ$ ), but is located at heliocentric distance of  $\sim 28 \text{ kpc}$ , on the other side of the Galaxy. The metallicity of  $-1.0$  dex of our feature is consistent with the range of metallicity of the stars in the Sagittarius stream. However, the expected heliocentric radial velocities of stars in the Sagittarius stream along our LOS is  $+180 \pm 15 \text{ km s}^{-1}$ ; the velocities of the stars in our feature are  $-36.5 \pm 8 \text{ km s}^{-1}$ . Thus we conclude that the cold kinematic feature that we detect is not associated with the Sagittarius stream. To confirm the existence of this stream and to better measure its properties will require additional spectroscopic observations over a larger field of view.

### 5.1. Comparison in Baade's Window

We compare our SMD in BW with Zoc08 and Fulbright et al. (2006) (Fb06 hereafter) in Figure 12. Our BW/bulge sample consists of 557 RCGs. The Zoc08 sample consists of 204 stars at the bright end of our RCG sample, and covers a very similar color range; their selection limits are indicated by the rectangle in Figure 1. They supplement their sample with 200 RCGs in BW (Lecureur et al. in prep.), but these latter measurements are not yet published so we

can only make comparison to the former sample. The Fb06 bulge sample is obtained by the recalibration of the Sadler et al. (1996) sample that consists of about 320 RCGs.

Because the individual uncertainties of our sample are large, we convolve Zoc08 and Fb06 SMDs with our error distribution to make consistent comparisons. We generate 10000 random realizations (with replacement) of the Zoc08 and Fb06 samples, and add to them an error distribution that is randomly drawn from our observed error distribution. The solid histogram in both panels of Figure 12 is our SMD, and the dashed histograms show the Zoc08 (left panel) and Fb06 (right panel) SMDs. We agree very well with both of these measurements. The major difference is an excess of stars around  $-0.90$  dex in our SMD, due to the cluster NGC 6522. Since the center of this cluster is only  $30''$  from the edge of our field, we include a significant number of cluster stars in our sample. The sample of Fb06 discriminates against cluster stars by construction (Terndrup et al. 1995) and the photometric limits of Zoc08 select only a small part of the cluster's red giant branch. Thus we expect our sample to include higher proportion of stars from this cluster. Our mean metallicity in BW is  $-0.09$  dex, close to solar, and agrees well with Zoc08 ( $\sim 0.0$  dex) and Fb06 ( $-0.10$  dex). Our dispersion in BW is  $0.58$  dex, comparable to the value of  $0.52$  dex calculated from the Fb06 sample. Both are larger than the dispersion of  $0.40$  dex measured by Zoc08.

### 5.2. Metallicity gradient along the Bar

The mean metallicity and dispersion are lower at the two offset positions in the bar compared to BW (see Table 1). Zoc08 and Minniti et al. (1995) find a gradient of about  $-0.25$  dex along the minor axis of the bar/bulge between  $b = -4^\circ$  and  $-12^\circ$ . We report here the first measurements of metallicity gradients along the major axis of the bar. We find a larger gradient towards  $l = +5^\circ$  ( $-0.45 \pm 0.05$  dex) than towards  $l = -5^\circ$  ( $-0.10 \pm 0.05$  dex). The metallicity dispersion is larger in BW as compared to the offset positions and decreases almost equally, by  $-0.20 \pm 0.05$  dex in each direction. This trend correlates with the LOS velocity dispersion that is also higher in BW and decreases by equal amounts at the offset positions as shown in Paper I. The higher mean metallicity at the center of bar may suggest that we are seeing an older, metal rich bulge population in BW compared to the stars at  $l = \pm 5^\circ$  in the bar.

## 6. DISCUSSION AND CONCLUSION

In this paper, we have presented EW measurements of the Ca II  $\lambda 8542$  line using FP absorption spectroscopy at three position along the major axis of the Galactic bar. This is the first attempt to use FP spectra for measuring stellar absorption line strengths. We show that reliable line strengths can be obtained for hundreds of stars with this technique, allowing future FP observations to measure accurate radial velocities and line strengths simultaneously from the same datacube.

We compare our CaT index with those of C04 and Ca07, and find that the major difference between them comes from the differences in the integration bandpass. This has a minor effect for weak lines but deviates non-linearly as the line strength increases, reflecting the strong damped wings of the CaT lines. We find the three indices to be tightly correlated, and the ratio of EW to its uncertainty remains constant for all of them. The differences between them does not affect any previous metallicity measurement, since each index was calibrated to  $[\text{Fe}/\text{H}]$  appropriately. We have investigated the effect of adding more samples to the FP data, and have found that the uncertainty of the EW can be reduced by a factor of two (i.e. to be comparable to the accuracy of similar S/N slit spectroscopy) by including as few as four extra samples on the red side of the absorption line (between  $8555 - 8580 \text{ \AA}$ ).

To test the reliability our EWs we derive the metallicity of NGC 6522, a bulge globular cluster that is present in our BW field. We used the C04 calibration to infer the metallicity from our EWs. We obtained mean  $[\text{Fe}/\text{H}]$  for this cluster to be  $-0.90$  dex, in excellent agreement with recent measurement from Zoc08. However, previous measurements of NGC 6522 have reported a relatively lower mean  $[\text{Fe}/\text{H}]$  of  $-1.28 \pm 0.12$  (Terndrup et al. 1998),  $-1.44 \pm 0.15$  (Zinn 1985) and  $-1.21 \pm 0.04$  (Rutledge et al. 1997), where the former two measurements were obtained using CMDs and the latter one used the CaT method. A relatively moderate mean metallicity is surprising for this cluster as it has a very blue horizontal branch. This cluster is most probably one of the 'second parameter' bulge clusters, where the metallicity is not the sole factor in determining the HB morphology (Catelan 2000; Fusi Pecci & Bellazzini 1997). The second parameter could be the age of the cluster, mass lost on the RGB, rotation, helium abundance, etc. The bulge sample of Zoc08 also contains five stars from another bulge globular cluster NGC 6558 for which a detailed analysis is presented in Barbuy et al. (2007). This bulge cluster was also found to be moderately metal poor ( $-0.97$  dex) with a very blue horizontal branch. Their analysis suggested that age was the second parameter for this cluster. They found it to be old at 14 Gyrs, and  $\alpha$ -enhanced. A complete chemical abundance analysis of NGC 6522 is being performed by the same group (Barbuy et al. in preparation). Any further analysis of second parameter issues in NGC 6522 is beyond the scope of this paper.

We use the EWs of 10 stars in our sample that also have high resolution  $[\text{Fe}/\text{H}]$  measurements to obtain the calibration between the EW of the Ca II  $\lambda 8542$  line and  $[\text{Fe}/\text{H}]$  for the RCGs in the Galactic bulge. We find this calibration to be marginally different from that of the globular clusters. We use this calibration to infer  $[\text{Fe}/\text{H}]$  for all the RCGs in our sample at three LOS in the bar to obtain the SMDs. The signature of NGC 6522 is detected in the BW SMD around  $-0.90$  dex. We find the mean metallicity in BW to be close to solar, consistent with previous work, and find a metallicity gradient that is different at positive ( $-0.45$  dex) and negative ( $-0.10$  dex) longitudes. The metallicity dispersion also shows gradient of about  $-0.20$  dex between BW and  $l = \pm 5^\circ$  LOS. Pérez et al. (2009) found that the bars in external galaxies can have positive, negative, or null metallicity gradients. They argue that these measurements can constrain the models of structure formation and star formation history for the inner parts disk galaxies, and may

also distinguish between a bar and a classical bulge. We expect that our measurements can similarly constrain models of the MW bar/bulge.

One would naturally expect that the metallicity gradient along the bar would be symmetric with respect to the center. We observe that the metallicity gradient is significantly different on the two sides of the bar. We do not know the origin of this difference. One possible reason would arise from extinction in the bar. The point of closest approach of the LOS to the Galactic center lies behind the bar in the first quadrant, but before the bar in the fourth quadrant. The density of the metal rich bulge population decreases rapidly with distance from the Galactic center. Thus if there is a significant amount of extinction within the bar, as is commonly seen in other galaxies, the LOS in the fourth quadrant will be more bulge-dominated than the LOS in the first quadrant. Thus while there would be a metallicity gradient on both LOS, the gradient in the first quadrant would be greater, as observed.

The velocity and metallicity distributions at  $l = +5.5^\circ$  show a distinct feature at  $-36.5 \text{ km s}^{-1}$  and  $-1.0 \text{ dex}$  respectively. This is a previously unknown cold kinematic feature, not associated with the Sagittarius stream. Spectroscopic observation over a larger FOV along this LOS are required to confirm this feature. This will be possible with our planned future survey of the bar.

We plan to use the FP system on the 10-m class Southern African Large Telescope (SALT) to obtain a much more extensive determination of the kinematics and metallicity of stars in the inner Galaxy. SALT's much greater aperture and larger FOV will enable us to measure  $\gtrsim 2000$  stars along a single LOS in an hour of observing time. We will investigate at least 10 LOS along the major axis of the bar, obtaining 15000 – 20000 stellar spectra in total. By slightly changing the observing strategy for scanning the absorption line we will obtain EW measurements of much higher precision than those of this paper. In addition we will select fields in BW that already have high-resolution [Fe/H] measurements to greatly improve the precision of the CaT to [Fe/H] calibration. Such a large sample of radial velocity and metallicities along several positions in the bar will be ideal to look for other cold kinematic features from disrupted satellites, gradients in the shape of velocity and SMDs, and correlations between them, and search for hypervelocity stars.

We thank Andrew Cole for his advice on the Calcium Triplet method and providing the 47 Tuc data, Michael Rich for his very useful comments and suggestions, Manuela Zoccali for confirming our NGC 6522 result, and Aaron Grocholski and Marta Mottini for their advice. Tad Pryor provided a wealth of suggestions and insights. Support was provided by Andrew Baker, Eric Gawiser and Saurabh Jha, and the National Science Foundation through grant AST0507323.

TABLE 1  
MEAN METALLICITY AND ITS DISPERSION, AND KINEMATICS OF THE RCGS IN THE BAR FOR THREE LOS.

LOS ( <i>l</i> , <i>b</i> )	$\langle [\text{Fe}/\text{H}] \rangle$ (dex)	$\sigma_{[\text{Fe}/\text{H}]}$ <sup>a</sup> (dex)	$\langle V_{\text{los}} \rangle$ km s <sup>-1</sup>	$\sigma_{V_{\text{los}}}$ <sup>a</sup> km s <sup>-1</sup>	N
(5.5,-3.5)	$-0.55 \pm 0.03$	$0.42 \pm 0.03$	$30.73 \pm 3.89$	$102.38 \pm 2.39$	738
(1.1,-3.9)	$-0.09 \pm 0.04$	$0.58 \pm 0.04$	$-1.01 \pm 5.42$	$112.62 \pm 3.41$	557
(-5.0,-3.5)	$-0.17 \pm 0.03$	$0.39 \pm 0.03$	$-52.56 \pm 3.85$	$102.30 \pm 2.50$	804

<sup>a</sup>The dispersion is measured using Maximum Likelihood Estimator

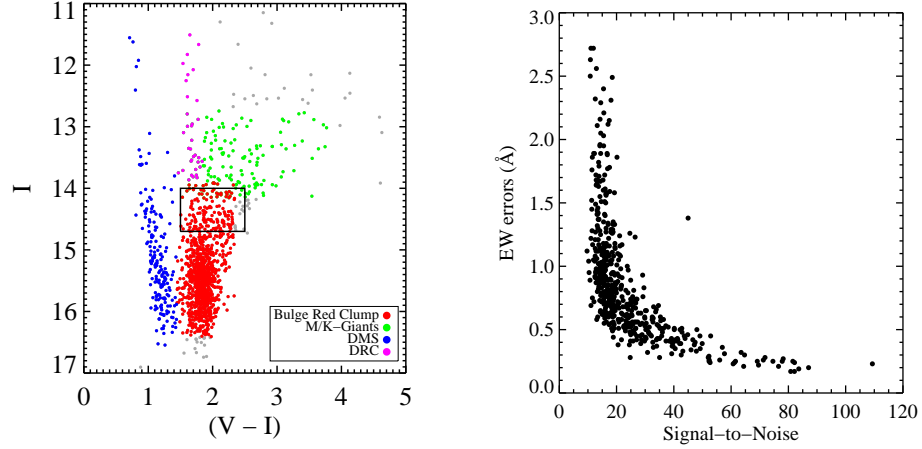


FIG. 1.— Left: CMD for (*l*, *b*) = (−5.0, −3.5) LOS. We have radial velocity and  $\text{EW}_{8542}$  for every star on this plot. CMDs at the other two LOS have similar features. The rectangle shows the bulge sample selection of Zoccali et al. (2007). The I and V band photometry comes from the OGLE survey. Right: EW uncertainties as a function of S/N for  $l = -5^\circ$  line-of-sight.



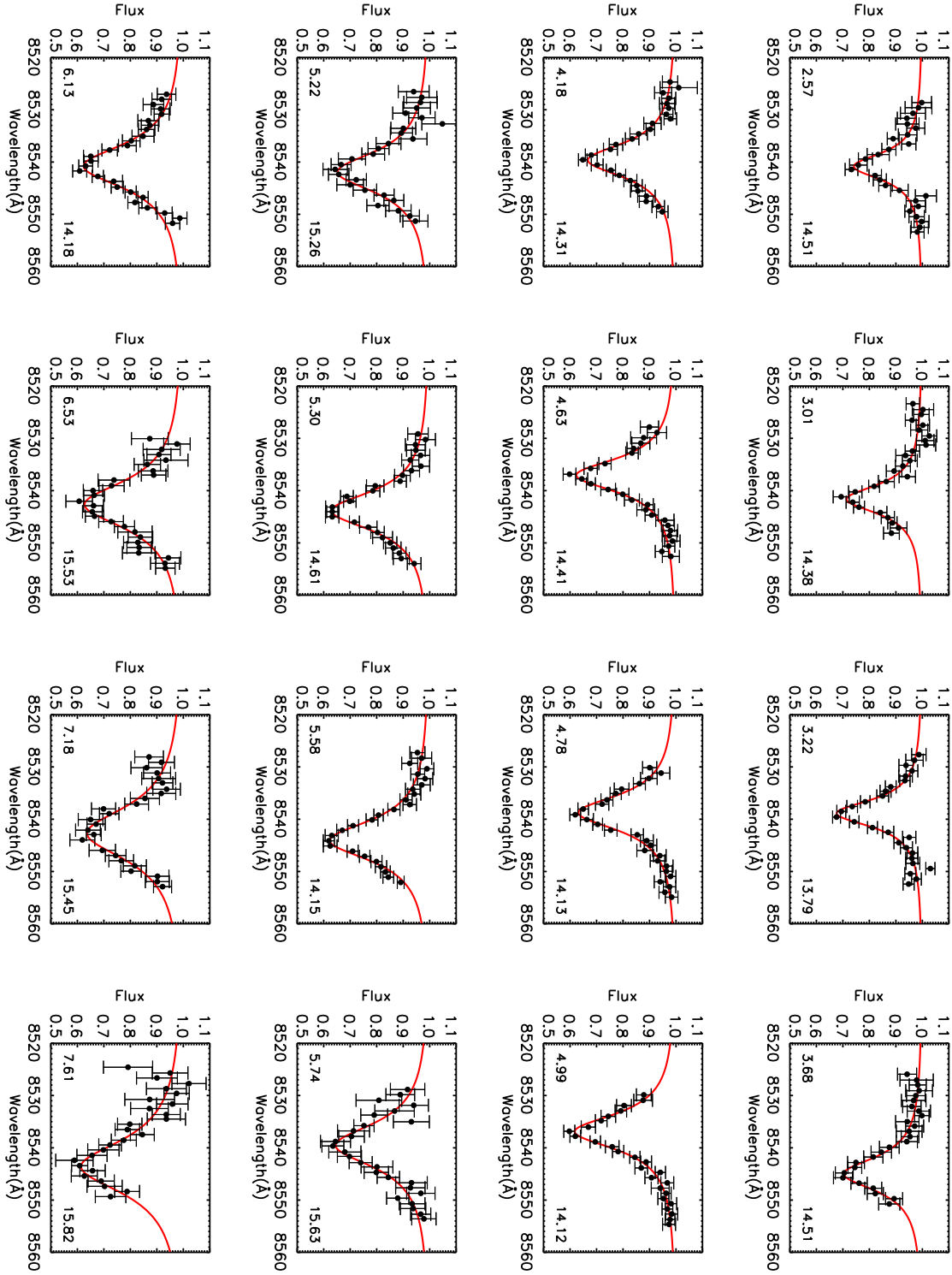


FIG. 2.— A sub-sample of Ca II  $\lambda 8542$  absorption lines illustrating the range of EWs measured. Solid line is the Voigt fit. EW (lower left) and I-band magnitude (lower right) are listed for each spectrum.

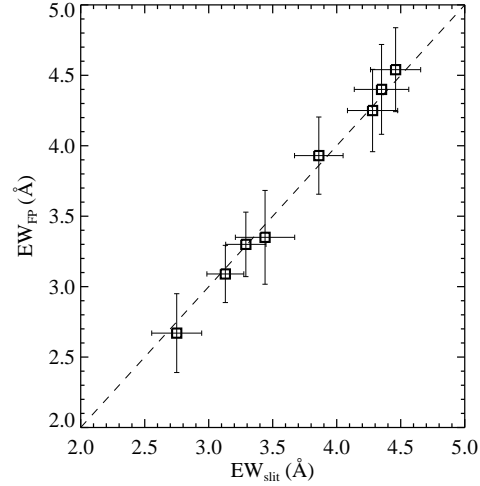


FIG. 3.— Comparing EWs of Ca II  $\lambda 8542$  line measured by fitting Voigt function to 25 Å bandpass (FP) and 60 Å bandpass (slit).

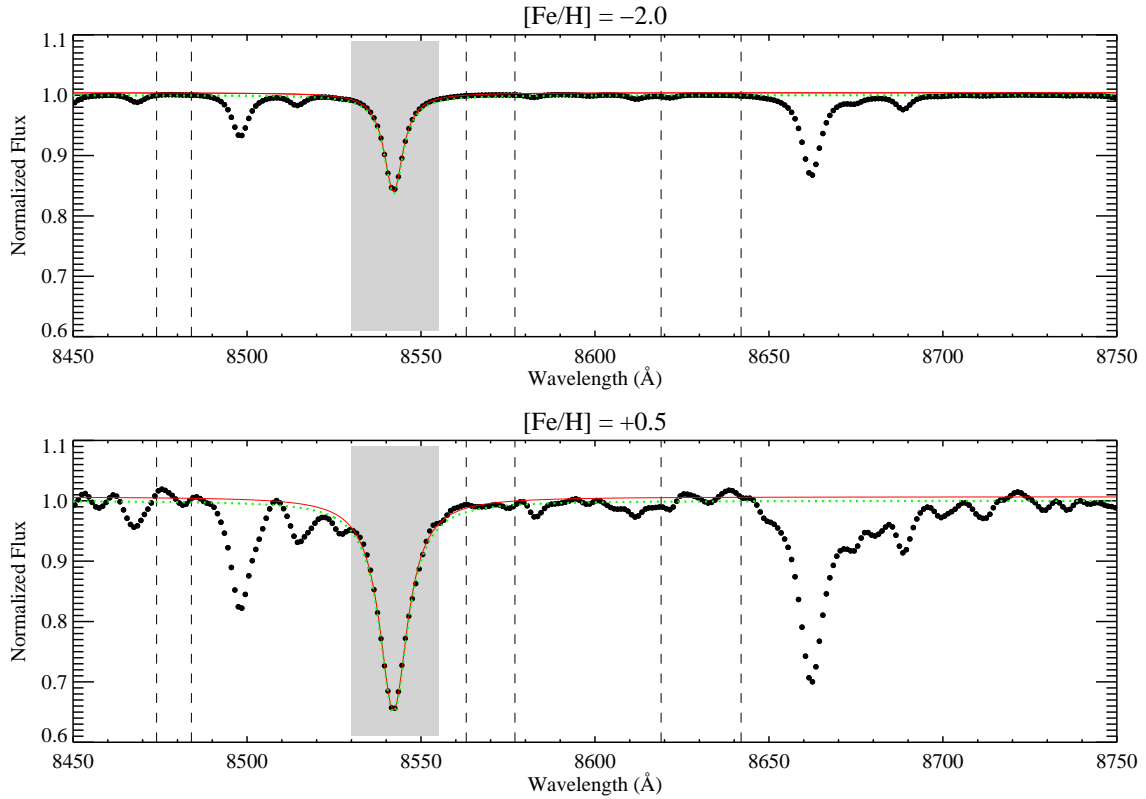


FIG. 4.— Synthetic spectra for two different metallicities are fit with a Voigt function using two different estimates of the continuum: (1) the continuum bands from Ca07 (red solid line) and (2) the continuum from the best-fit Voigt function (green dotted line). The shaded region shows the range (8530 Å – 8555 Å) over which we fit the Voigt function to our FP spectra. Vertical dashed lines show Ca07 continuum bands.

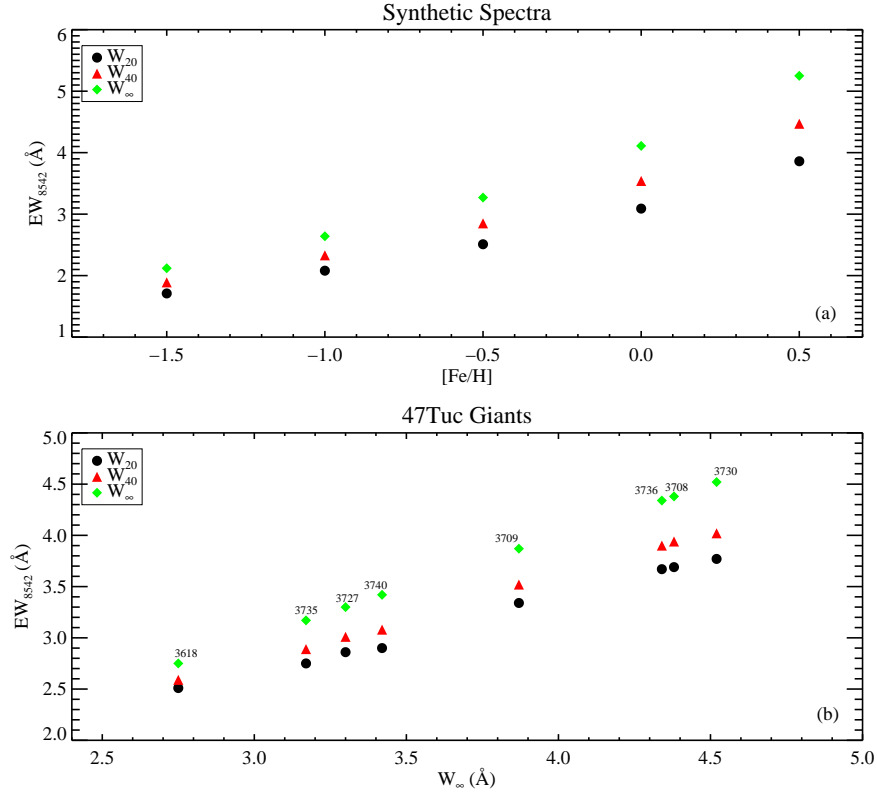


FIG. 5.— Top panel:  $W_{\infty}$ (diamonds),  $W_{40}$  (triangles) and  $W_{20}$  (circles) are measured using synthetic spectra and plotted as a function of  $[Fe/H]$ . Bottom panel: The three indices are plotted as a function of  $W_{\infty}$  using spectra of 8 red giant stars from 47 Tuc. The points are labeled with the star ID.

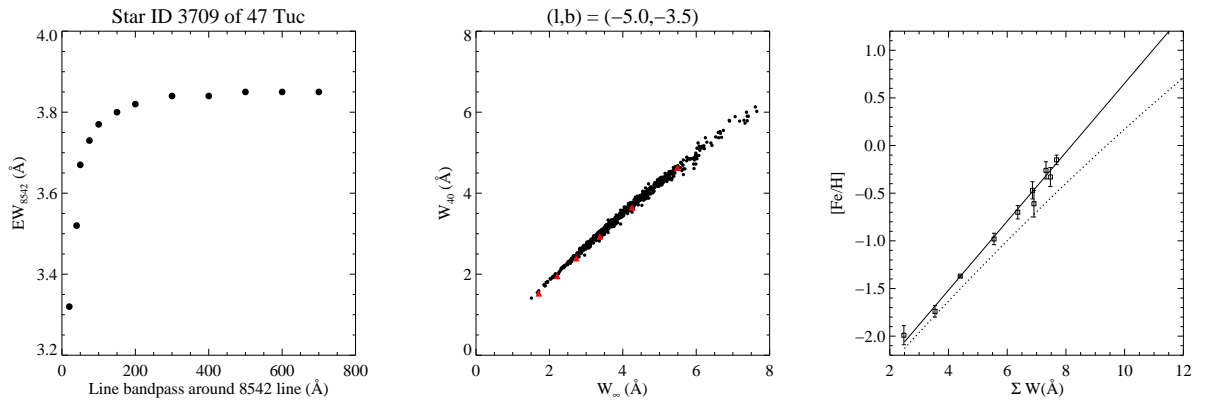


FIG. 6.— Left panel: EW as a function of line bandpass. Middle panel:  $W_{\infty}$  and  $W_{40}$  for our sample at  $l = -5$ . Red points are from synthetic spectra. Right Panel: Solid line: calibration of C04's index for a sample of globular clusters; dotted line: Calibration curve transformed to our index  $W_{\infty}$ .

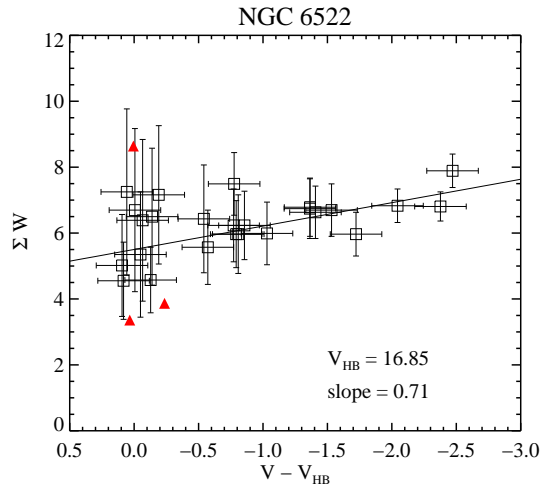


FIG. 7.— The summed EW varies linearly with V band magnitude. The solid line is the best linear fit. Red triangles indicate excluded stars.

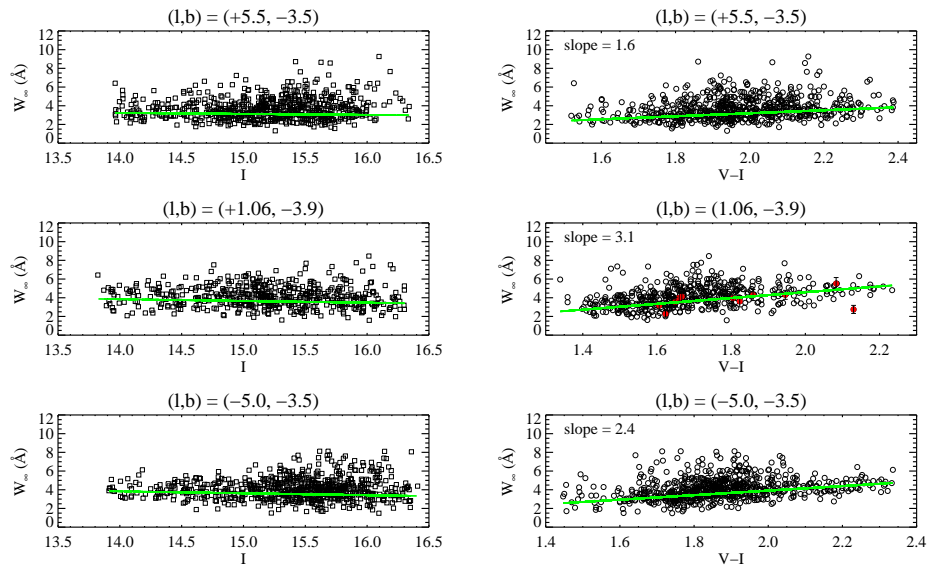


FIG. 8.—  $W_{\infty}$  as a function of color and I-band magnitude. The solid line is the best straight-line fit. Calibration stars indicated in red.

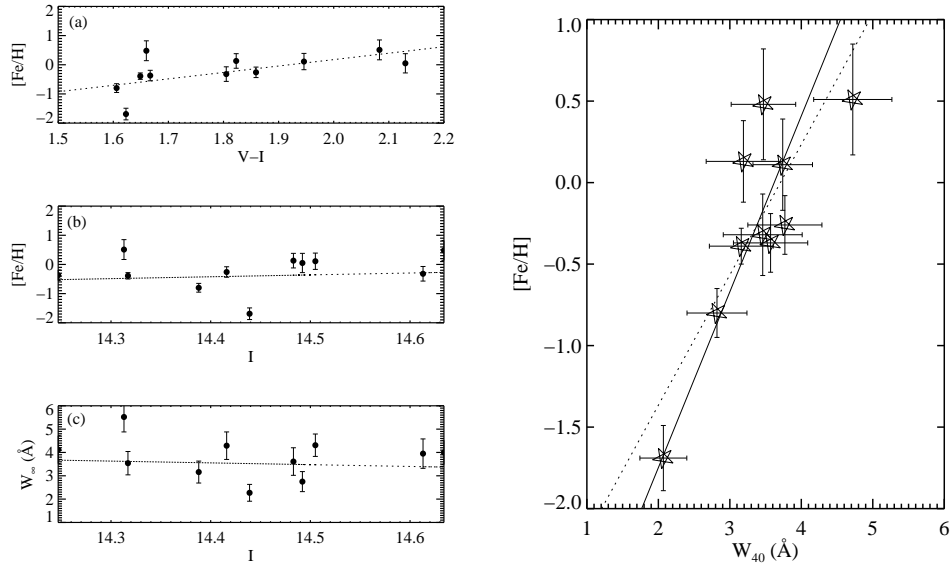


FIG. 9.— Left panel: (a)  $[\text{Fe}/\text{H}]$  as a function of V-I color; (b) I magnitude ; (c) EW as a function of I-band magnitude for the 10 calibration stars. Right panel: Calibration between  $[\text{Fe}/\text{H}]$  and CaT for the bulge RCGs.

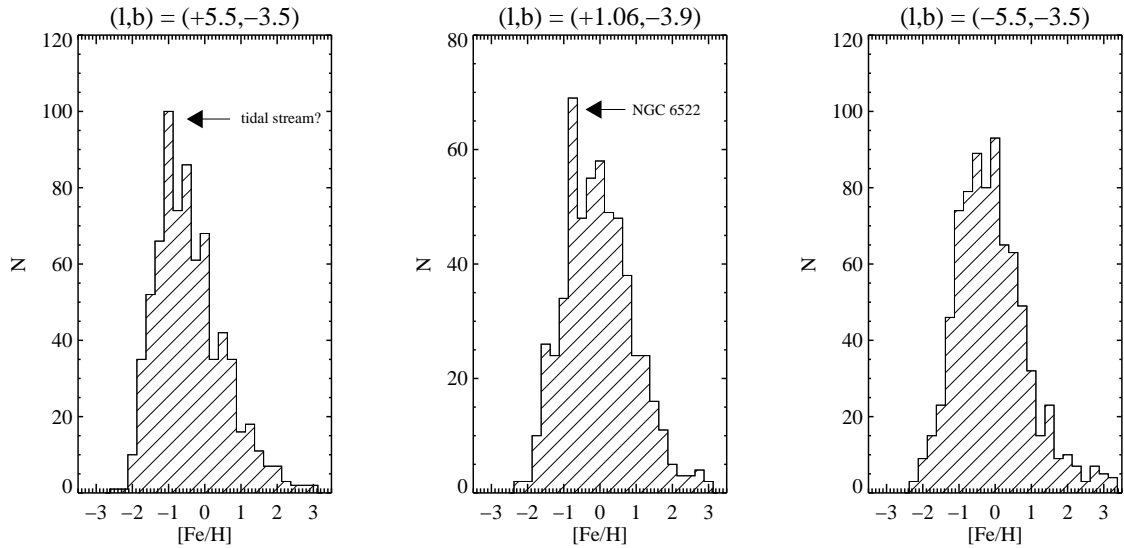


FIG. 10.— SMDs along the major axis of the bar.

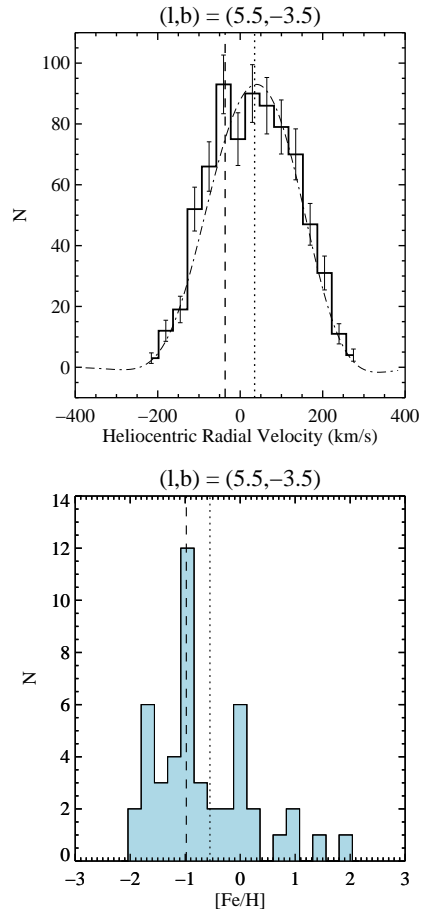


FIG. 11.— Possible signature of disrupted satellite: top panel: the velocity distribution of 738 stars, with an excess around  $-35 \text{ km s}^{-1}$ ; bottom panel: the metallicity distribution of 47 stars in this velocity excess, selected with radial velocity between  $-45 \text{ km s}^{-1}$  and  $-28 \text{ km s}^{-1}$ . In both panels the dotted line indicates the mean of the distribution and the dashed line indicates the location of the excess.

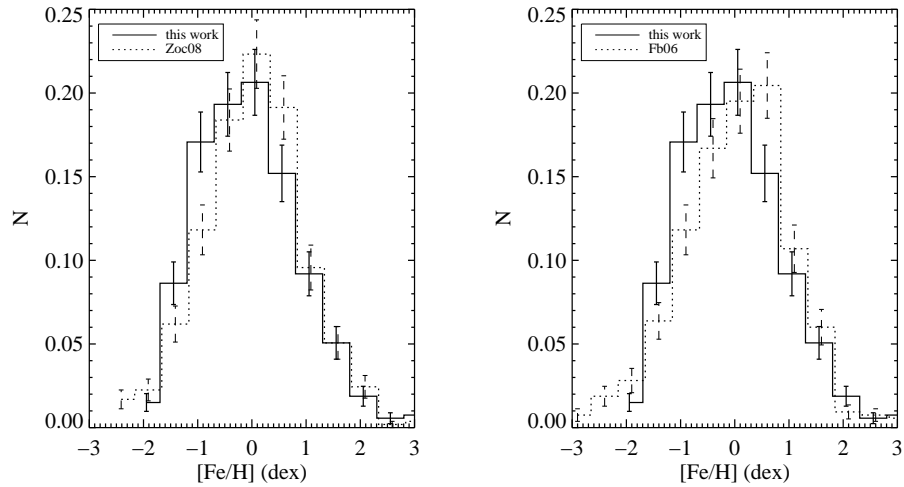


FIG. 12.— Comparing the stellar metallicity distributions to previous work in Baade's Window.

## REFERENCES

- Alcock, C., Allsman, R. A., Alves, D. R., Axelrod, T. S., Becker, A. C., Bennett, D. P., Cook, K. H., Drake, A. J., Freeman, K. C., Geha, M., Griest, K., Lehner, M. J., Marshall, S. L., Minniti, D., Nelson, C. A., Peterson, B. A., Popowski, P., Pratt, M. R., Quinn, P. J., Stubbs, C. W., Sutherland, W., Tomaney, A. B., Vandehei, T., & Welch, D. L. 2000, *ApJ*, 541, 734
- Armandroff, T. E., & Da Costa, G. S. 1991, *AJ*, 101, 1329
- Armandroff, T. E., & Zinn, R. 1988, *AJ*, 96, 92
- Ballero, S. K., Matteucci, F., Origlia, L., & Rich, R. M. 2007, *A&A*, 467, 123
- Barbuy, B., Zoccali, M., Ortolani, S., Minniti, D., Hill, V., Renzini, A., Bica, E., & Gómez, A. 2007, *AJ*, 134, 1613
- Carrera, R., Gallart, C., Pancino, E., & Zinn, R. 2007, *AJ*, 134, 1298
- Catelan, M. 2000, *ApJ*, 531, 826
- Cenarro, A. J., Cardiel, N., Gorgas, J., Peletier, R. F., Vazdekis, A., & Prada, F. 2001, *MNRAS*, 326, 959
- Cole, A. A., Smecker-Hane, T. A., Tolstoy, E., Bosler, T. L., & Gallagher, J. S. 2004, *MNRAS*, 347, 367
- Dwek, E., Arendt, R. G., Hauser, M. G., Kelsall, T., Lisse, C. M., Moseley, S. H., Silverberg, R. F., Sodroski, T. J., & Weiland, J. L. 1995, *ApJ*, 445, 716
- Erdelyi-Mendes, M., & Barbuy, B. 1989, *A&AS*, 80, 229
- Freudenreich, H. T. 1998, *ApJ*, 492, 495
- Fulbright, J. P., McWilliam, A., & Rich, R. M. 2006, *ApJ*, 636, 821
- 2007, *ApJ*, 661, 1152
- Fusi Pecci, F., & Bellazzini, M. 1997, in *The Third Conference on Faint Blue Stars*, ed. A. G. D. Philip, J. Liebert, R. Saffer, & D. S. Hayes, 255–+
- Howard, C. D., Rich, R. M., Reitzel, D. B., Koch, A., De Propriis, R., & Zhao, H. 2008, *ApJ*, 688, 1060
- Ibata, R. A., Gilmore, G., & Irwin, M. J. 1995, *MNRAS*, 277, 781
- Jones, J. E., Alloin, D. M., & Jones, B. J. T. 1984, *ApJ*, 283, 457
- Majewski, S. R., Kunkel, W. E., Law, D. R., Patterson, R. J., Polak, A. A., Rocha-Pinto, H. J., Crane, J. D., Frinchaboy, P. M., Hummels, C. B., Johnston, K. V., Rhee, J., Skrutskie, M. F., & Weinberg, M. 2004, *AJ*, 128, 245
- Martínez-Delgado, D., Gómez-Flechoso, M. Á., Aparicio, A., & Carrera, R. 2004, *ApJ*, 601, 242
- Matteucci, F. 1992, *Memorie della Societa Astronomica Italiana*, 63, 301
- Minniti, D., Olszewski, E. W., Liebert, J., White, S. D. M., Hill, J. M., & Irwin, M. J. 1995, *MNRAS*, 277, 1293
- Minniti, D., & Zoccali, M. 2008, 245, 323
- Mould, J. R. 1976, *ApJ*, 210, 402
- Munari, U., Sordo, R., Castelli, F., & Zwitter, T. 2005, *A&A*, 442, 1127
- Pérez, I., Sánchez-Blázquez, P., & Zurita, A. 2009, *A&A*, 495, 775
- Piotto, G., King, I. R., Djorgovski, S. G., Sosin, C., Zoccali, M., Saviane, I., De Angeli, F., Riello, M., Recio-Blanco, A., Rich, R. M., Meylan, G., & Renzini, A. 2002, *A&A*, 391, 945
- Pryor, C., & Meylan, G. 1993, 50, 357
- Rangwala, N., Williams, T. B., & Stanek, K. Z. 2009, *ApJ*, 691, 1387
- Rich, R. M. 1988, *AJ*, 95, 828
- Rich, R. M., Howard, C., Reitzel, D. B., Zhao, H., & de Propriis, R. 2007, *ArXiv e-prints*, 710
- Rutledge, G. A., Hesser, J. E., & Stetson, P. B. 1997, *PASP*, 109, 907
- Sadler, E. M., Rich, R. M., & Terndrup, D. M. 1996, *AJ*, 112, 171
- Smith, G., & Drake, J. J. 1988, *MNRAS*, 231, 115
- Sosin, C., Piotto, G., Djorgovski, S. G., King, I. R., Rich, R. M., Dorman, B., Liebert, J., & Renzini, A. 1997, in *Stellar Ecology: Advances in Stellar Evolution*, 92–95
- Stanek, K. Z., Udalski, A., Szymanski, M., Kaluzny, J., Kubiak, M., Mateo, M., & Krzeminski, W. 1997, *ApJ*, 477, 163
- Stetson, P. B. 1987, *PASP*, 99, 191
- Sumi, T., Wu, X., Udalski, A., Szymański, M., Kubiak, M., Pietrzyński, G., Soszyński, I., Woźniak, P., Żebruń, K., Szweczyk, O., & Wyrzykowski, L. 2004, *MNRAS*, 348, 1439
- Szymanski, M. K. 2005, *Acta Astronomica*, 55, 43
- Terndrup, D. M., Popowski, P., Gould, A., Rich, R. M., & Sadler, E. M. 1998, *AJ*, 115, 1476
- Terndrup, D. M., Sadler, E. M., & Rich, R. M. 1995, *AJ*, 110, 1774
- Tolstoy, E. 2005, 118
- Weiner, B. J., & Sellwood, J. A. 1999, *ApJ*, 524, 112
- Zhao, G., Qiu, H. M., & Mao, S. 2001, *ApJ*, 551, L85
- Zinn, R. 1985, *ApJ*, 293, 424
- Zoccali, M., Hill, V., Lecureur, A., Barbuy, B., Renzini, A., Minniti, D., Gómez, A., & Ortolani, S. 2008, *A&A*, 486, 177
- Zoccali, M., Lecureur, A., Barbuy, B., Hill, V., Renzini, A., Minniti, D., Momany, Y., Gómez, A., & Ortolani, S. 2007, 241, 73
- Zoccali, M., Renzini, A., Ortolani, S., Greggio, L., Saviane, I., Cassisi, S., Rejkuba, M., Barbuy, B., Rich, R. M., & Bica, E. 2003, *A&A*, 399, 931